

Two-dimensional Classical Wigner Crystal: Elliptical Confining Potential

Zhen-zhong Zhang and Kai Chang

NLSM, Institute of Semiconductors, Chinese Academy of Sciences, P.O. Box 912, Beijing 100083, China

We investigate theoretically the ground-state configurations of two-dimensional charged-particle systems with an elliptical hard-wall boundary and their vibrational eigenmodes. The system exhibits a series of structural transitions, finally changing from a zigzag structure to a one-dimensional Coulomb chain, as the eccentricity of the elliptical hard-wall boundary is increased.

PACS numbers: 52.27.Lw, 36.40.Sx, 82.70.Dd

I. INTRODUCTION

In 1934, Wigner predicted that electrons will crystallize in a three-dimensional electron gas and form a lattice when the density of the gas is lowered to a certain critical value. Since then, Wigner crystals have been observed in various low-dimensional systems. These systems include electrons on the surface of liquid helium [1], electrons confined in semiconductor quantum dots [2], colloidal suspensions with microscopic particles [3], vortices in superfluids [4], and strongly coupled dusty plasma [5].

Recently, classical Wigner crystals have aroused considerable interest both experimentally [6, 7, 8, 9, 10] and theoretically [11, 12, 13, 14, 15]. Theoretical results for the ground-state configurations and normal mode spectra of classical Wigner crystals agree with experiments very well. Very recently, Melzer observed experimentally [9] that a two-dimensional (2D) charged-particle system under an anisotropic parabolic confining potential forms a one-dimensional (1D) chain through a zigzag transition, which agrees with the theoretical expectation [11, 15]. Most previous studies have focused on systems under a parabolic confining potential or Coulomb potential induced by a fixed positive charge. There have been only a few investigations of isotropic hard-wall confinement [14, 16]. These have adopted Monte Carlo simulation augmented with the Newton optimization technique. Since Newton optimization cannot directly minimize the energy of a system under the hard-wall confining potential, the authors [14] adopted an r^n -like confinement to simulate hard-wall confinement in order to study the static and dynamical properties, because an r^n -like potential approaches the hard-wall confining potential when the exponent n approaches the infinity.

In this paper, we adopt a nonlinear optimization algorithm (L-BFGS-B) [17] to investigate the ground-state configuration of a 2D charged-particle system under an elliptical hard-wall confining potential. The excitation modes for different shapes of confining potential are also studied. The present paper is organized as follows. In Sec. II, our model and numerical method are introduced.

In Sec. III, we calculate the ground-state configurations and find that they exhibit a series of structural phase transitions as the anisotropy of the elliptical hard-wall boundary is increased. Sec. IV describes the influence of the anisotropy of the hard-wall confining potential on the normal mode excitation spectrum. Finally, our conclusions are given in Sec. V.

II. THEORETICAL MODEL

The potential energy of a 2D system of N charged particles including the Coulomb potential under a hard-wall confining potential $V_c(r)$ is given by

$$= \sum_{i=1}^N (V_c(r_i) + \frac{q^2}{4\pi\epsilon_0} \sum_{i>j} \frac{1}{|\mathbf{r}_i - \mathbf{r}_j|}) \quad (1)$$

In the case of an elliptical hard-wall confining potential, utilizing the coordinate transform $x_i = r_i \cos \theta_i$; $y_i = e r_i \sin \theta_i$, where e refers to the eccentricity of the elliptical boundary, the elliptical hard-wall confining potential can be expressed as

$$V_c(r) = \begin{cases} 0 & \text{if } r < R_c \\ 1 & \text{if } r \geq R_c \end{cases}; \quad (2)$$

where R_c is the major axis length.

By choosing $r_0 = R_c$ as the unit of length and $E_0 = q^2/(4\pi\epsilon_0 R_c)$ as the unit of energy, the potential energy in dimensionless form is

$$= \sum_{i>j}^N \frac{1}{(r_i \cos \theta_i - r_j \cos \theta_j)^2 + e^2 (r_i \sin \theta_i - r_j \sin \theta_j)^2} \quad (3)$$

where $0 \leq r_i, r_j < 1$; $0 \leq \theta_i, \theta_j < 2\pi$: From this form, we note that the Hamiltonian depends only on the number of particles N and the eccentricity e of the elliptical boundary. Due to the invariance of the system configuration after a $\pi/2$ rotation, we only investigate the cases of $0 \leq e \leq 1$ in this paper.

The L-BFGS-B algorithm [17], which is an improved version of the BFGS [18] algorithm, can find the minimum of a function $f(\mathbf{r}; \mathbf{x}_1; \mathbf{x}_2; \dots; \mathbf{x}_n)$ under the constraint of $l_i \leq x_i \leq u_i$: To solve the boundary

Electronic address: kchang@red.semi.ac.cn

problem, we obtain the piece-wise linear path $x(t) = P(x_i, t; l; u)$ by projecting the steepest descent direction onto the feasible region:

$$P(x; l; u) = \begin{cases} l_i & \text{if } x_i < l_i \\ x_i & \text{if } x_i \in [l_i, u_i] \\ u_i & \text{if } x_i > u_i \end{cases} \quad (4)$$

Such a transformation enables us to find the local minimum of the univariate piece-wise quadratic $q_n(t) = y_n(x(t))$, in which x^c is defined as the Cauchy point. The variables whose value at x^c is at the lower or upper bound, comprising the active set $A(x^c)$, are held fixed. Then we consider the following problem:

$$\min (x : x_i = x_i^c; \forall i \in A(x^c)) \quad (5)$$

$$l_i \leq x_i \leq u_i \quad \forall i \notin A(x^c) \quad (6)$$

First, adopting the conjugate gradient algorithm [18] on the subspace of free variables, we approximately solve Eq. (5). In the iterative process, we take x^c as the initial value for iteration, and then truncate the path to satisfy Eq. (6). After an approximate solution \bar{x}_{n+1} has been obtained, f decreases further along $d_n = \bar{x}_{n+1} - x_n$ on the condition that x_{n+1} is in the appropriate range (boundary constraint). Then the approximation Hessian matrix and the gradient vector at x_{n+1} are calculated, and a new iteration starts. Such iterations continue until the required accuracy is achieved. More detailed information about this algorithm can be found in Ref. [17].

The total energy of the system under the elliptical hard-wall confining potential (see Eq. (3)) can be minimized by the L-BFGS-B algorithm. First, all particle coordinates are generated randomly. Secondly, the L-BFGS-B algorithm is adopted to minimize the total energy of the system. We repeat the above procedure many times. Finally, we choose the configuration with the lowest energy as the ground-state of the system. To check the accuracy and validity of this algorithm, we reproduced the ground-state configurations for an isotropic hard-wall potential [14].

Once the system ground-state is obtained, the vibrational eigenmode can be calculated by diagonalizing the dynamical matrix (see Appendix). The eigenfrequencies in this paper are expressed in the unit $\omega_0 = \sqrt{E_0/(m r_0^2)}$.

III. NUMERICAL RESULTS AND DISCUSSIONS

A. The ground-state configuration

When the charged particles are confined by a hard-wall potential, they repel each other due to the Coulomb interaction so that some particles first move to the boundary until the outer shell is fully occupied, the remaining

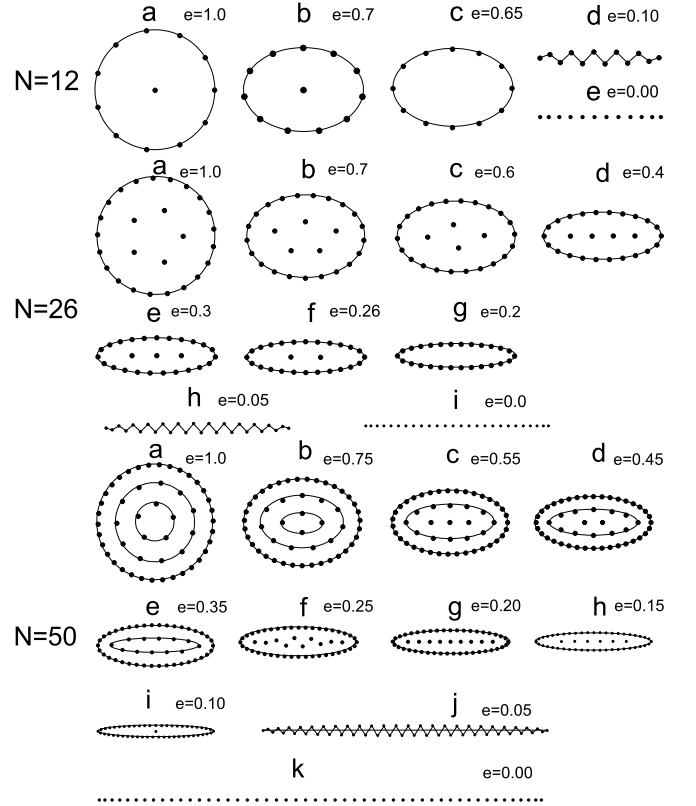


FIG. 1: The ground state configurations of three clusters with different numbers of particles $N = 12, 26, 50$ for different eccentricities of the elliptical boundary.

particles stay in the inner shells. The shape of the boundary significantly affects the system ground-state configuration. Fig.1 shows the evolution of the ground-state configurations for different numbers of particles as the boundary eccentricity e decreases. The ground-state configurations in the anisotropic case are quite different from those in the isotropic case ($e = 1$). They change significantly with decreasing eccentricity e , and exhibit zigzag structures when e approaches zero.

Taking the $N = 50$ cluster as an example, we can find a continuous deformation from circular to elliptical rings as the eccentricity e decreases. The inner ring collapses into a line with decreasing e . Notice that more and more particles leave the central line and merge into the adjacent outer ring. Then the system forms two elliptical rings (see Fig. 1). This process repeats until the system exhibits a quasi-one-dimensional zigzag configuration and becomes a straight line at $e = 0$. In addition, inner shells are more sensitive to the change of the eccentricity e than outer shells. Decreasing e further, particles in the inner shell move to the outer shell, and the inner shell finally collapses into a line.

We find that there are two different kinds of transitions: slow and abrupt transitions. For convenience, we refer to the configuration in which $N - 1$ particles are on the outer shell and one at the centre as α -type, and the

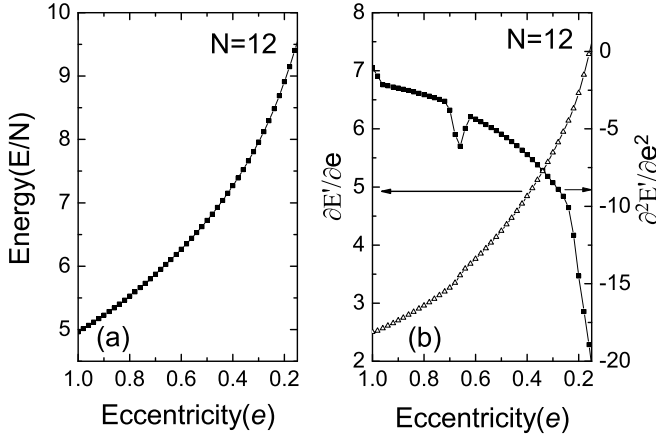


FIG. 2: The ground-state energies, the first derivative and second derivative of the ground state energy with respect to the eccentricity as a function of the eccentricity for $N = 12$.

configuration in which all particles are on the outer shell as α -type. From the Table I in Ref. [14], we know that the system exhibits the α -type configuration for $N = 12$ under a circular hard-wall confining potential. But for an elliptical confining potential, the transition from α -type to β -type occurs as the boundary eccentricity e decreases to a certain value. Fig. 2 (a) shows the system energy of $N = 12$ as a function of the eccentricity e when the major axis is fixed and the minor axis decreases with e . When e decreases and the area is compressed, the total energy increases. We adopt $E^0 = E|_{e^2}$ and calculate the first and second derivatives of E^0 with respect to e , i.e. $\partial E^0/\partial e$; $\partial^2 E^0/\partial e^2$, which are shown in Fig. 2 (b). An obvious dip in $\partial^2 E^0/\partial e^2$ appears with the decrease of e . As seen in Fig. 1, the system ground-state is α -type at $e = 0.7$ and β -type at $e = 0.65$. The transition from α -type to β -type takes place at $e = 0.666, 0.546$, and 0.483 respectively for $N = 12, 13$, and 14 .

In Figs. 3 and 4, we plot the second derivative of energy with respect to the eccentricity e for $N = 26$ and 50 as a function of eccentricity e . More transitions, which are denoted by the vertical lines, can be found. From the evolution of three clusters, the ground-state configurationally transits from α -type to β -type and finally to a 1D chain through a zigzag structure. Note how the system evolves from 2D to 1D. In Fig. 5 (a) and 5 (b), we plot zigzag angles and particle density of zigzag structures and a 1D chain as a function of particle position for $N = 50$. From Fig. 5 (a), we find the density per unit length of a 1D chain ($e = 0$) exhibits behavior similar to that of the zigzag structure as the x coordinate increases. It remains almost constant in the central region and increases significantly at the edges of the chain. These behaviors of a 1D chain under hard-wall confinement are very different from those under a parabolic potential, which was investigated by Dubin. [21] and Melzer [9].

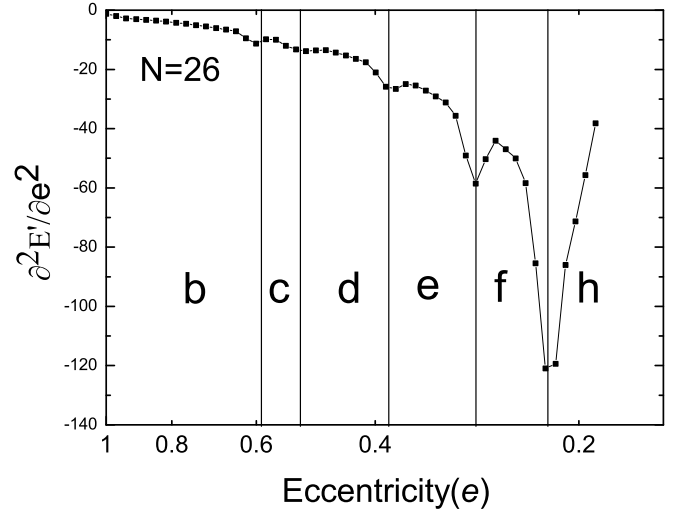


FIG. 3: The second-order derivative $\partial^2 E^0/\partial e^2$ as a function of eccentricity for $N = 26$, where b-h correspond to the configurations for $N = 26$ in Fig.1

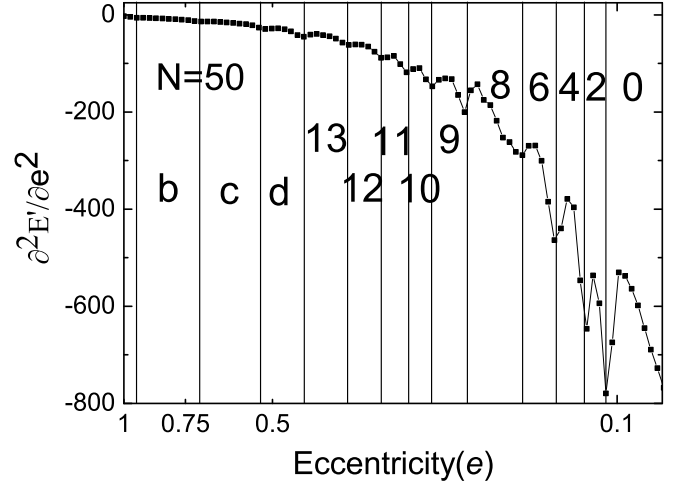


FIG. 4: Same as Fig.3, but for $N = 50$. The numbers denote the number of particles in the inner shell.

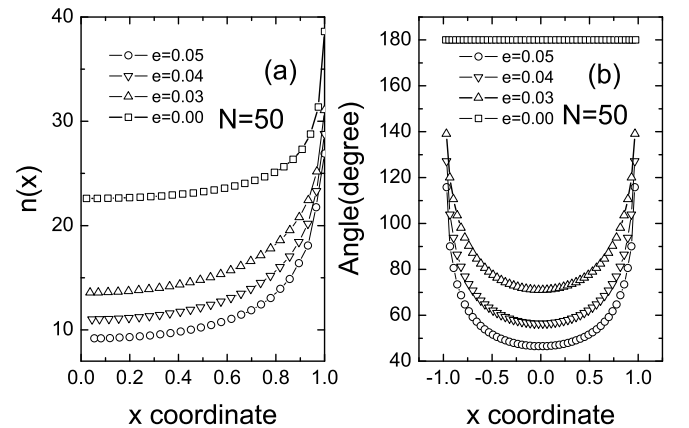


FIG. 5: Density per unit length $n(x)$, and zigzag angle as a function of coordinate x for different eccentricities.

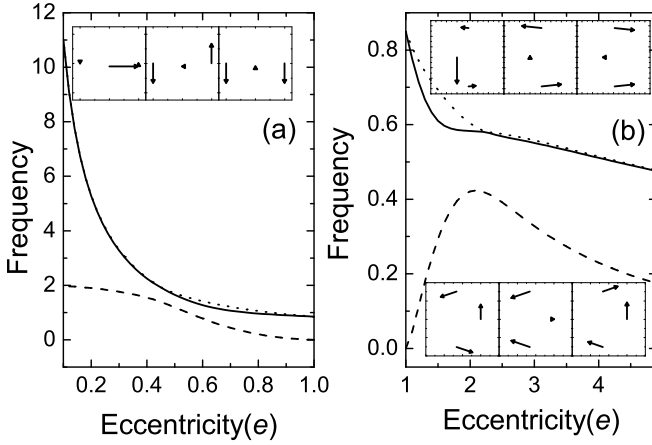


FIG. 6: The frequency spectra as functions of the eccentricity e for a cluster $N = 3$. The dashed, solid, and dotted lines denote the frequencies of three vibrational modes. The eigenvectors, with frequencies arranged in ascending order from left to right, are in the insets in Fig. 6(a) for $e = 0.1$. The eigenvectors of $e = 1.6$ are in the lower insets of Fig. 6(b), and those of $e = 2.8$ are in the upper insets of Fig. 6(b).

IV. THE EIGENMODE SPECTRUM

In this section, we discuss the vibrational modes of the ground state under the elliptical hard-wall confining potential.

Because the radial motion of the particles at the boundary is practically frozen, only $2N - N_E$ modes exist when the N_E particles are located at the boundary. But under elliptical hard-wall confinement, the rotational mode with zero frequency at $e = 0$ becomes nonzero and some degenerate modes split due to the breaking of cylindrical symmetry. In addition, increasing the eccentricity e results in abrupt transitions of the ground-state configurations ($N = 12$), and their eigenmodes change significantly because of the abrupt change of the number of particles at the boundary.

A. $N = 3$ particle cluster

The frequencies of three vibrational modes in an $N = 3$ cluster as a function of eccentricity e are shown in Figs. 6(a) and 6(b). One can find two different mechanisms driving the transition of the ground state configuration as the anisotropy increases. One is due to anisotropic hard-wall confinement. The other is the minor (major) axis of the ellipse decreases (increases), and consequently the Coulomb interaction increases (decreases) for $e < 1$ ($e > 1$). When e approaches 1, the former mechanism is dominant and the rotational mode frequency increases (see dashed line in Fig. 6(b)). In addition, this mechanism makes high-frequency (HF) degenerate mode split into two modes (see Fig. 6(a,b) solid and dotted lines). When e decreases (increases) further, the latter mechanism

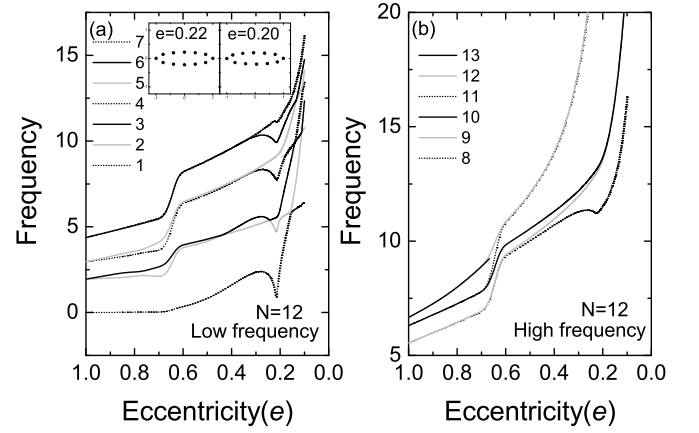


FIG. 7: The frequency spectra as functions of the eccentricity e for a cluster $N = 12$.

becomes more important, and two split HF modes degenerate approximately again and the low-frequency (LF) mode saturates gradually. From the eigenvectors at $e = 0.1$ (see the insets of Fig. 6(a)), we find that decreased eccentricity e enhances the confinement along the y axis, and consequently leads to the increases of frequencies of the vibration modes along the y axis. Thus those frequencies tend to infinity in the extreme case of $e = 0$. From the 1D Coulomb chain potential function, we diagonalize the dynamical matrix of the ground-state configuration for an $N = 3$ cluster and get that the lowest frequency is 2.0 and the two high frequencies are infinity, which agrees with Fig. 6(a). In addition, Figs. 6(a) and 6(b) show that the two split modes cross respectively at $e = 2.3$ and 0.44 (notice $2.3 - 1 = 0.44$). We compare the eigenvector of the highest frequency at $e = 1.6$ with that at $e = 2.8$ (see the insets of Fig. 6(b)). One can see that two particles near the major axis move in the same direction at $e = 1.6$ but in the opposite direction at $e = 2.8$. This verifies that the cross occurs indeed between $e = 1.6$ and $e = 2.8$.

B. $N = 12$ particle cluster

In this subsection we discuss a larger system ($N = 12$) to illuminate the effect of the elliptical hard-wall boundary on the spectrum of the system. Fig. 7 shows all eigenfrequencies of the $N = 12$ cluster as a function of the eccentricity e . From this figure, we see that the frequency spectra exhibit many jumps between $e = 0.668$ to $e = 0.6$. This is because the system transits from $-$ type to $+$ type at $e = 0.666$ (see the definition of $-$ type and $+$ type in Section II). The distance between neighboring particles decreases, resulting in an abrupt increase of the eigenfrequency. In addition, the highest frequency mode diminishes due to the freezing of the radial motion of all particles at the boundary (see the thirteenth mode in Fig. 7(b)). It is interesting to note that a small

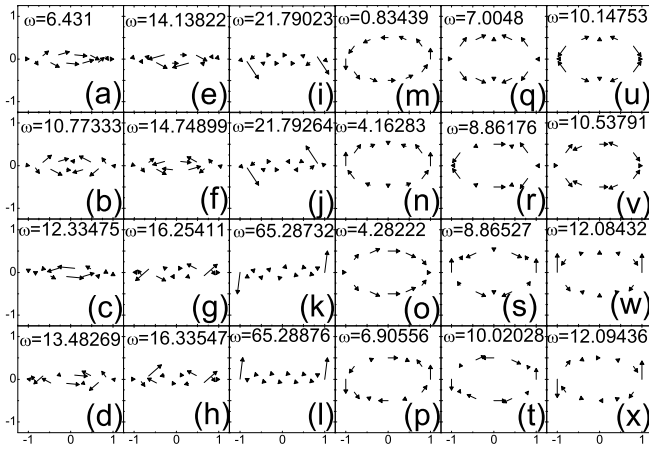


FIG. 8: All eigenvector for the clusters with $N = 12$ particles at $e = 0.1$ and $e = 0.5$. (a-l) is for $e = 0.1$ and (m-x) is for $e = 0.5$

dip appears at $e = 0.22$ which cannot be found in the energy curve of the system (see Fig. 2). Checking the ground-state configuration around $e = 0.22$, we find that the system changes from α -type to the zigzag structure (see the insets in Fig. 7(a)). Next, we explain the effect of the elliptical boundary on vibrational modes in detail in three regions.

When $e < 0.66$, the system ground state configuration is α -type, and there are thirteen vibrational modes. Among these modes, the anisotropic effect results in the apparent splitting of the LF modes, but the effect on the other higher frequency modes is negligible.

When $0.22 < e < 0.66$, the system ground state configuration is β -type. Because the number of particles increases by one at the boundary, and the HF modes recompose due to the configuration transition from α -type to β -type. As the eccentricity e decreases, the second mode crosses with the third mode (see Fig. 7(a)). A similar feature was observed experimentally in an anisotropic parabolic confinement [9]. In the HF part (see Fig. 7(b)), the ninth mode departs from the eighth mode and becomes degenerate with the tenth mode gradually, corresponding to the slow transition of the configuration.

When $e < 0.22$, the system ground-state configuration is a zigzag structure. From the inset in Fig. 7, we find that the zigzag structure destroys the configuration symmetry, resulting in the splitting of the degenerate modes in the isotropic hard-wall confining potential. The lowest vibrational mode is no longer the rotation mode, and more crosses between LF modes (see Fig. 7(a)) can be found. The LF eigenvectors at $e = 0.1$ and $e = 0.5$ show clearly the crosses of different modes. From the eigenvectors of the $N = 12$ cluster in Fig. 8, we can compare the vibration direction of eigenmodes at $e = 0.1$ with that at $e = 0.5$ and find that all corresponding particles move in the same way among the vibrational modes (a) and (o), (b) and (q), (c) and (m), (d) and (r). The particles with larger vibration amplitudes in the LF modes

appear close to the center of the system as e decreases. But the behavior of the HF modes is opposite to that of the LF modes (see Fig. 8).

V. CONCLUSION

The ground-state configuration and dynamical properties of a 2D classical cluster of charged particles in an elliptical hard-wall confining potential are investigated theoretically. The dependence of the ground-state configuration on the number of particles and the eccentricity of the confining potential are discussed in detail. As the eccentricity e decreases, the system exhibits two different kinds of transitions, i.e., slow and abrupt transitions. When increasing the system anisotropy, circular shells are deformed into ellipses continuously, the inner shell collapses into a line, and then number of particles in the line decreases gradually. Last, the system exhibits a zigzag structure and forms a 1D Coulomb chain when e approaches zero.

The boundary anisotropy significantly influences the frequency of the vibrational modes. With increasing the anisotropy of the boundary, the rotation mode becomes nonzero and degenerate modes split due to the breaking of cylindrical symmetry. The rotation mode is no longer the lowest vibrational mode when the eccentricity e approaches zero.

Acknowledgments

This work was supported by the NSFC Grant No. 60376016, 60525405.

*

In this appendix, we present the dynamical matrix of a 2D classical system under the elliptical coordinates. Using the coordinate transformation, $x_i = e_i \cos \theta_i$; $y_i = e_i \sin \theta_i$, where e denotes the eccentricity of the elliptical hard-wall boundary, one can obtain $\underline{x} = e \cos \theta$ and $\underline{y} = e \sin \theta$. The equilibrium positions of the particles are denoted by

$$\begin{pmatrix} x_i \\ y_i \end{pmatrix} = \begin{pmatrix} e_i \cos \theta_i \\ e_i \sin \theta_i \end{pmatrix}.$$

In the harmonic approximation around the equilibrium position, the Lagrangian can be expressed as $L(\underline{f}_i; \underline{g}_i; \underline{f}_i; \underline{g}_i) = \frac{1}{2} m \sum_i (\dot{\underline{f}}_i^2 + \dot{\underline{g}}_i^2) + \frac{1}{2} \sum_{i,j} (f_i^2 \cos^2 \theta_i + \sin^2 \theta_i) + \frac{1}{2} \sum_{i,j} (e^2 \sin^2 \theta_i + \cos^2 \theta_i) \frac{1}{r_{ij}} + 2 \sum_{i,j} (1 - e^2) \sin \theta_i \cos \theta_j$; where

$$r_{ij} = \sqrt{(x_i - x_j)^2 + (y_i - y_j)^2}; \quad \underline{f}_i = \begin{pmatrix} f_i \cos \theta_i \\ f_i \sin \theta_i \end{pmatrix}; \quad \underline{g}_i = \begin{pmatrix} g_i \cos \theta_i \\ g_i \sin \theta_i \end{pmatrix}; \quad \underline{f}_{ij} = \left(\frac{\partial^2}{\partial \theta_i \partial \theta_j} \right)_{eq};$$

$\underline{g}_{ij} = \left(\frac{\partial^2}{\partial \theta_i \partial \theta_j} \right)_{eq}$; etc. Since $\theta_i \neq 0$; linearizing the equation of motion for \underline{f}_i and \underline{g}_i and defining $\underline{T} = \begin{pmatrix} \underline{f}_i & \underline{g}_i \end{pmatrix}$, we can obtain the equation of the particles' movement under matrix form $\frac{d^2}{dt^2} \underline{T} = \underline{M}^{-1} \underline{T}$. So the dynamical matrix of a 2D classical system \underline{M}

is $\frac{\begin{smallmatrix} B & G \\ A & C & B & D \\ A & G \\ B & D & A & C \end{smallmatrix}}{\begin{smallmatrix} C & E \\ A & C & B & D \\ B & E \\ B & D & A & C \end{smallmatrix}} \frac{\begin{smallmatrix} B & H \\ A & C & B & D \\ A & H \\ B & D & A & C \end{smallmatrix}}{\begin{smallmatrix} C & F \\ A & C & B & D \\ B & F \\ B & D & A & C \end{smallmatrix}},$ where

$$\begin{aligned} \mathbb{A}_{ij} &= (e^2 \cos^2 \frac{0}{i} + \sin^2 \frac{0}{i}); \mathbb{B}_{ij} = (1 - e^2) \sin \frac{0}{i} \cos \frac{0}{i}; \\ \mathbb{C}_{ij} &= (e^2 \sin^2 \frac{0}{i} + \cos^2 \frac{0}{i}); \mathbb{D}_{ij} = (1 - e^2) \sin \frac{0}{i} \cos \frac{0}{i}; \end{aligned}$$

$$\begin{aligned} \mathbb{E}_{ij} &= \frac{i}{j}; \mathbb{F}_{ij} = \frac{-\frac{i}{0} \frac{j}{j}}{j}; \mathbb{G}_{ij} = \frac{-\frac{i}{0} \frac{j}{i}}{i}, \text{ and} \\ \mathbb{H}_{ij} &= \frac{-\frac{i}{0} \frac{j}{0}}{\frac{0}{i} \frac{0}{j}}. \end{aligned}$$

-
- [1] C.C. Grimes and G. Adams, Phys. Rev. Lett. 42, 795 (1979).
- [2] R.C. Ashoori, H.L. Stormer, J.S. Weiner, L.N. Pfeiffer, S.J. Pearton, K.W. Baldwin, and K.W. West, Phys. Rev. Lett. 68, 3088 (1992).
- [3] R. Bubeck, C. Bechinger, S. Nesser and P. Leiderer, Phys. Rev. Lett. 82, 3364 (1999)
- [4] Y. Kondo, J.S. Korhonen, M. Korusius, V.V. Dmitriev, E.V. Thuneberg, and G.E. Volovik, Phys. Rev. Lett. 68, 3331 (1992)
- [5] J.H. Chu and Lin I, Phys. Rev. Lett. 72, 4009 (1994)
- [6] A. Melzer, M. K lindworth, and A. Piel, Phys. Rev. Lett. 87, 115002 (2001)
- [7] M. Golbovsky, Y. Saado, and D. D avidov, Phys. Rev. E. 65, 061405 (2002)
- [8] A. Melzer, Phys. Rev. E. 67, 016411 (2003)
- [9] A. Melzer, Phys. Rev. E. 73, 056404 (2006)
- [10] M. Saint Jean, C. Even and C. Guthmann, Europhys. Lett. 55, 45 (2001)
- [11] J.P. Schi er, Phys. Rev. Lett. 70, 818 (1993)
- [12] J.A. D rocco, C. J.O lson Reichhardt, C. Reichhardt, and B. Janko, Phys. Rev. E. 68, 060401 (2003)
- [13] Hiroo Totsuji, Tokunari Kishimoto, Chieko Totsuji, and Kenji Tsuruta, Phys. Rev. Lett. 88, 125002 (2002)
- [14] M. Kong, B. Partoens, A. Matulis, and F.M. Peeters, Phys. Rev. E. 69, 036412 (2004)
- [15] L. Candido, J.P. Rino, N. Studart and F.M. Peeters, J. Phys.: Condens. Matter. 10, 11627 (1998)
- [16] V.M. Bedanov and F.M. Peeters, Phys. Rev. B 49, 2667 (1994)
- [17] R.H. Byrd, P. Lu and J. Nocedal, SIAM Journal on Scientific and Statistical Computing. 16, 1190 (1995)
- [18] W.H. Press, B.P. Flannery, S.A. Teukolsky, and W.T. Vetterling, Numerical Recipes (Cambridge University Press Cambridge, England, 1986)
- [19] V.A. Schweigert and F.M. Peeters, Phys. Rev. B. 51, 7700 (1995)
- [20] E. Polak, Computational Methods in Optimization (Academic, New York, 1971).
- [21] H.E. Dubin, Phys. Rev. E. 55, 4017 (1997)